This article has been accepted for publication in a future issue of this journal, but has not been fully edited. Content may change prior to final publication. Citation information: DOI 10.1109/TNSRE.2019.2936383, IEEE Transactions on Neural Systems and Rehabilitation Engineering

Heuristic-Based Ankle Exoskeleton Control for Co-Adaptive Assistance of Human Locomotion

Rachel W. Jackson and Steven H. Collins, *Member, IEEE*

***Abstract*—Assisting human locomotion with exoskeletons is challenging, largely due to the complexity of the neuromusculoskeletal system, the time-varying dynamics that accompany motor learning, and the uniqueness of every individual's response to device assistance. Assistance strategies designed to keep the human "in-the-loop" can help overcome many of these challenges. The purpose of this study was to develop a human-in-the-loop assistance strategy that uses co-adaptive control to slowly and continuously respond to biomechanical changes thought to encode the user's needs. Online measurements of muscle activity and joint kinematics were used to guide the evolution of an exoskeleton torque pattern based on the following heuristics: 1) muscle activity that acts cooperatively with the exoskeleton indicates the user wants more torque; 2) muscle activity that acts antagonistically to the exoskeleton indicates the user wants less torque; and 3) torque should stop increasing if the user is not adapting. We applied our controller to tethered, bilateral ankle exoskeletons worn by naïve participants as they walked on a treadmill at 1.25 m·s^{-1} for 30 minutes. The evolved torque profiles reduced the root-mean-square of soleus muscle activity by $35 \pm 12\%$ and metabolic rate by $22 \pm 8\%$ compared to walking with the exoskeletons while they provided no torque. This was equivalent to a $9 \pm 12\%$ reduction in metabolic rate when compared to normal walking. Furthermore, the algorithm was responsive to changes in each user's coordination patterns. These results confirm the effectiveness of the controller and suggest a new approach to exoskeleton assistance aimed at fostering co-adaptation with the user. This technique might particularly benefit individuals with age-related muscle weakness.**

***Index Terms*—Exoskeleton, adaptation, gait, assistance, muscle activity.**

I. Introduction

EXOSKELETONS have the potential to enhance mobility in able-bodied individuals [1]–[7] and restore mobility to those with reduced functionality, such as the elderly [8], those with spinal cord injury [9], [10], or those with neurological disorders [10]–[12]. For decades, however, researchers struggled to design exoskeletons that achieved improvements in human performance comparable to those predicted by models of human walking [13]–[16] or expected based on an understanding of the mechanics and energetics of human movement [17]–[19]. The challenge stemmed, in large part, from the complexity and redundancy of the human motor control system. Coordination strategies adopted during walking with an exoskeleton are often unique to an individual and evolve over time [4], [20]–[22] making it difficult to know how individual users will respond to a given pattern of assistance and what pattern of assistance is best. Furthermore, the task of walking with exoskeleton-applied assistance is difficult and users, especially naïve users, often struggle to discover effective ways of interacting with assistive devices.

Human-in-the-loop optimization is a promising approach for overcoming many of these complexities, given its ability to customize assistance patterns for each user and facilitate motor learning. Human-in-the-loop optimization updates exoskeleton assistance in real time in response to measured changes in the user so as to maximize human performance [6], [23], [24]. We previously demonstrated the efficacy of human-in-the-loop optimization by using an evolutionary algorithm to identify ankle exoskeleton assistance parameters that minimized metabolic rate [6]. Other researchers had similar success using Bayesian optimization to find the optimal assistance parameters for a hip exoskeleton [24]. These methods achieved significant improvements in walking economy for their respective devices and the results from these studies suggest that it is important to keep the human 'in-the-loop' when developing assistance strategies.

Human-in-the-loop optimization has many advantages, but the development of alternative human-in-the-loop strategies may be beneficial for different populations, devices, and situations. For instance, to find optimal assistance parameters, human-in-the-loop optimization forces users to walk with a wide variety of torque patterns, many of which are suboptimal. Although such enforced exploration of different coordination strategies may be beneficial for motor learning [25], users must endure walking with uncomfortable torque patterns for sustained periods of time. Additionally, once assistance parameters are optimized, they are often held fixed even though users may still be changing their coordination patterns. Control techniques that, instead, prioritize continuous responsiveness and co-adaptation between the device and the user could address these issues.

One example of continuously-updated assistance is proportional myoelectric control, which provides device torque in direct proportion to measured muscle activity, thereby giving users step-to-step control over device assistance [20], [21], [26]. Incorporating an adaptive gain into the control scheme improved performance outcomes [4], further suggesting the importance of time-varying and customized assistance strategies. The update law, however, required maximum exoskeleton torque be applied on every walking step, thereby assuming the ideal level of assistance is known. Proportional myoelectric control, with or without an adaptive gain, inherently constrains the pattern of torque to match that of muscle activity on each step, permits large step-to-step fluctuations in torque resulting

R. W. Jackson is with the Department of Mechanical Engineering, Carnegie Mellon University, Pittsburgh, PA, USA and the Department of Bioengineering, Stanford University, Stanford, CA, USA (email: rwj1@stanford.edu).

S. H. Collins is with the Department of Mechanical Engineering, Carnegie Mellon University, Pittsburgh, PA, USA and the Department of Mechanical Engineering, Stanford University, Stanford, CA, USA.

This article has been accepted for publication in a future issue of this journal, but has not been fully edited. Content may change prior to final publication. Citation information: DOI 10.1109/TNSRE.2019.2936383, IEEE Transactions on Neural Systems and Rehabilitation Engineering

from inherent step-to-step variability in electromyography patterns, and does not account for indications of maladaptation, such as co-contraction or significant kinematic changes. These features may make it challenging for users to learn how to best utilize assistive devices.

The goal of this project was to develop an alternative human-in-the-loop assistance strategy that uses heuristics about effective human-device interaction to guide the discovery of an exoskeleton assistance pattern. Muscle activity that acts cooperatively with the exoskeleton may indicate that the user wants more assistance and could act to increase torque from the exoskeleton. Significant antagonistic muscle activity and large deviations from nominal joint kinematics may indicate that the user is having difficulty adapting to assistance and could act to slow or reverse growth of exoskeleton torque. Together, these measurements could be used to enable co-adaptation, in which the user and the device continuously respond and adapt to each other. We hypothesized that such an assistance strategy would improve whole-body locomotor economy in naïve exoskeleton users and allow the exoskeleton to adjust to the changing needs of each user. We expect such co-adaptive control strategies to help with the discovery of assistance techniques for new lower-limb devices and enhance our ability to assist people with a broad range of physiological needs, especially the elderly.

II. Algorithm Development

We developed a heuristic-based algorithm that uses real-time measurements of muscle activity and joint kinematics to guide the evolution of an ankle exoskeleton torque pattern (Fig. 1). The algorithm is based upon three main heuristics: 1) soleus muscle activity, which acts cooperatively with the ankle exoskeleton, indicates the user wants more torque; 2) tibialis anterior muscle activity, which acts antagonistically to the exoskeleton, indicates the user wants less torque; and 3) significant deviations from nominal ankle kinematics and a lack of reduction in gross measures of soleus muscle activity indicate that the user is having trouble adapting to exoskeleton-applied torque, therefore torque growth should slow or stop. We formulated a control scheme to best realize these driving heuristics and implemented it on tethered, bilateral ankle exoskeletons.

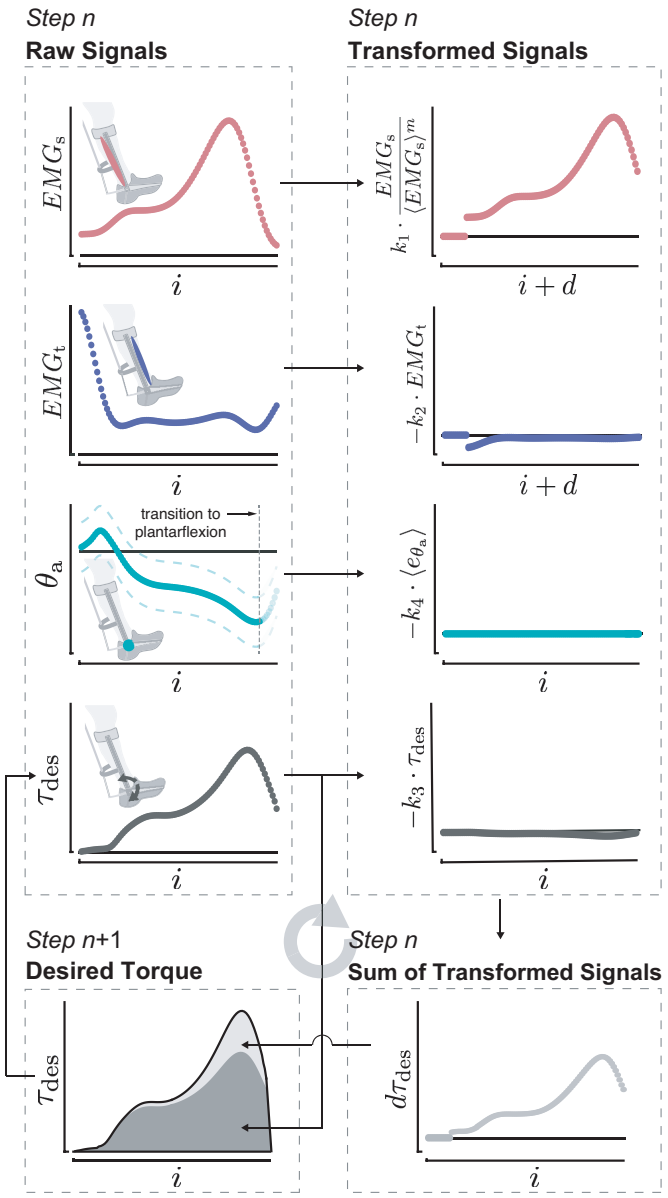

Fig. 1. Algorithm schematic. Soleus muscle activity (EMG_s), tibialis anterior muscle activity (EMG_t), ankle joint angle (θ_a), and desired exoskeleton torque (τ_{des}) measured on step n, at each sample i, are transformed and summed to produce the change in desired torque ($d\tau_{des}$). The change in desired torque ($d\tau_{des}$) is then added to the desired torque (τ_{des}) on step n to produce the desired torque on the next step, $n+1$.

A. Algorithm Formulation

On the first walking step, $n = 1$, exoskeleton torque, $\tau_{des}(i,n)$, is set to zero for all time indices, i. Exoskeleton torque then grows on each subsequent walking step, $n+1$, according to the following formula. The exoskeleton torque pattern on the next walking step, $\tau_{des}(i,n+1)$, is a linear combination of the current exoskeleton torque, $\tau_{des}(i,n)$, and a specified change in torque, $d\tau_{des}(i,n)$, calculated from measurements of the user's current biomechanics (Eq. 1). The contribution of current exoskeleton torque to torque on the next walking step adds a memory component to the control scheme. This prevents exoskeleton torque from being solely governed by the current coordination pattern of the user and enables exoskeleton torque to grow gradually over time. The change in torque is made up of contributions from soleus muscle activity, tibialis anterior muscle activity, ankle kinematics, and the magnitude of current exoskeleton torque (Eq. 2).

Soleus muscle activity at every time index, offset by time delay d to account for the neuromuscular and actuation delays between muscle activation and force production, $EMG_s(i+d,n)$, positively contributes to exoskeleton torque. The proportion of soleus muscle activity added to the exoskeleton torque profile is governed by two factors: the magnitude of the gain k_1 and the average soleus muscle activity over the current walking step, $\langle EMG_s(n) \rangle$. Average soleus muscle activity serves as a gross measure of how active the soleus muscle was over an entire walking step and is used as a

This article has been accepted for publication in a future issue of this journal, but has not been fully edited. Content may change prior to final publication. Citation information: DOI 10.1109/TNSRE.2019.2936383, IEEE Transactions on Neural Systems and Rehabilitation Engineering

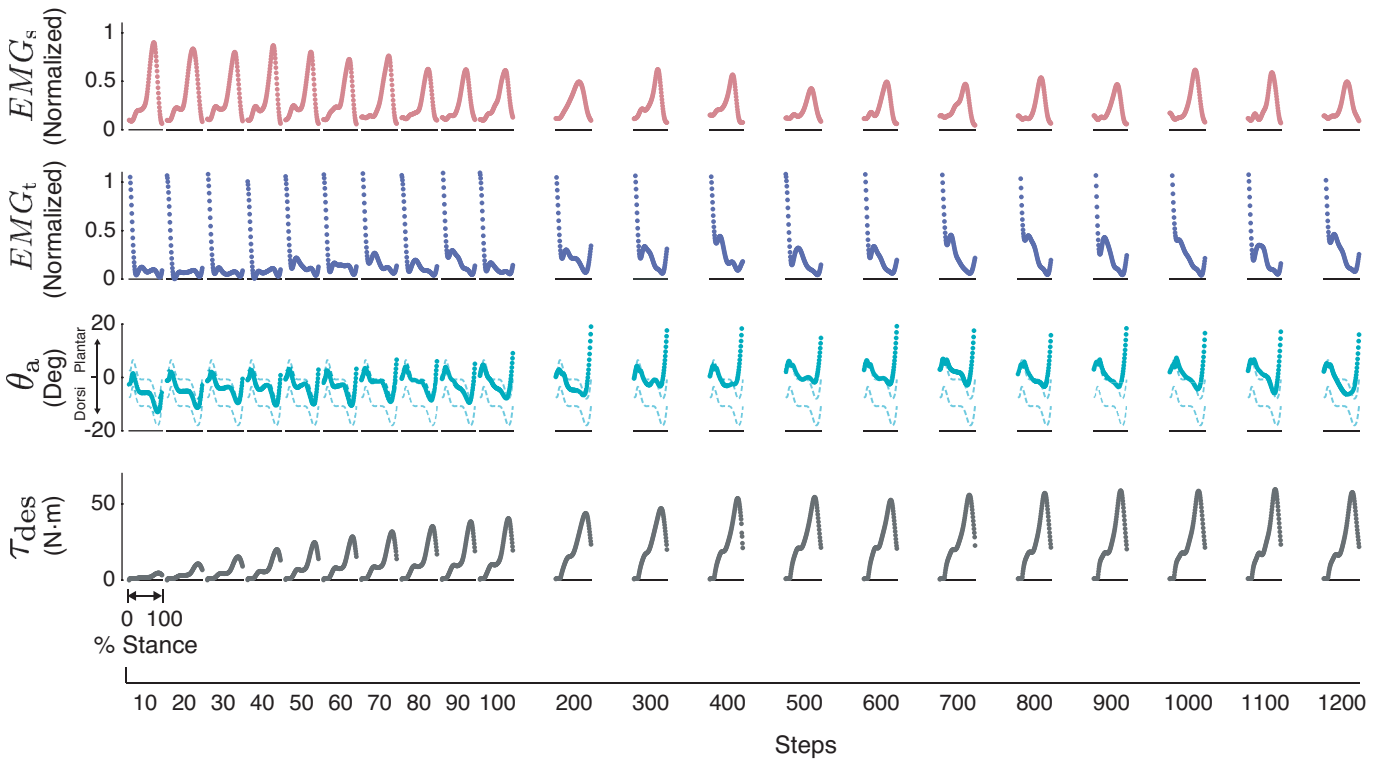

Fig. 2. Example of the co-adaptation that occurred between the user and the exoskeleton over time. Soleus muscle activity (EMG_s, *first row*), tibialis anterior muscle activity (EMG_t, *second row*), and ankle kinematics (θ_a, *third row*) guided the slow and responsive growth of ankle exoskeleton torque (τ_{des}, *last row*). As exoskeleton torque evolved, the patterns of soleus muscle activity, tibialis anterior muscle activity, and ankle kinematics changed in response to the applied torque, which in turn affected the torque profile on subsequent steps. Soleus and tibialis anterior muscle activity were normalized to peak muscle activity measured during walking in the Zero-Torque mode. The green, dashed lines around the ankle angle trajectory show the deadband around deviations in ankle kinematics. Each trajectory is shown as a percent of stance and plotted over time in steps. Up to 100 steps, trajectories are the average of 10 steps, after which trajectories are the average of 100 steps. Data presented is for the left leg of one participant.

proxy for user adaptation. High average soleus muscle activity over a walking step, even with low soleus muscle activity at specific time indices, suggests that the user needs more time to adapt. Therefore, high values of average muscle activity act to decrease the proportion of soleus muscle activity added to the torque pattern, while low values of average muscle activity act to increase the proportion of soleus muscle activity added to the torque pattern. By including this term, the controller is able to automatically speed up or slow down torque growth, depending on how well users seem to be adapting. The magnitude of the exponent m affects the relative contributions of average soleus muscle activity and soleus muscle activity at a specific time index to the growth rate of torque.

Three factors negatively contribute to the desired exoskeleton torque profile to help prevent desired torque from growing unstably: 1) tibialis anterior muscle activity at every delayed time index, $EMG_t(i+d,n)$; 2) average deviations in ankle kinematics from nominal over the dorsiflexion phase of gait, $\langle e_{\theta_a}(n)\rangle$; and 3) current exoskeleton torque at every time index, $\tau_{des}(i,n)$. The proportion of tibialis anterior muscle activity that contributes to exoskeleton torque is governed by the magnitude of the gain k_2. Without this term, the user may adopt a coordination strategy that relies heavily on co-contraction. The contribution of average ankle angle deviation to exoskeleton torque is governed by the magnitude of the gain k_4. Average ankle angle deviations must first reach a defined threshold, c_{θ_a}, which lies outside the range of natural step-to-step variations in ankle kinematics, so that only excessive deviations induced by exoskeleton-applied torque contribute to the torque profile. This term only acts to shift the entire torque pattern up or down. Initial attempts to incorporate kinematic deviations at every time index led to oscillatory torque patterns, likely due to delays between the applied force and measured changes in ankle angle. Without a term that incorporates kinematic changes, the user could adapt to the applied exoskeleton torque by walking with a more plantarflexed ankle joint, instead of reducing soleus muscle activity. Sustained levels of soleus muscle activity would continue to add to the exoskeleton torque pattern, leading to unconstrained growth. The negative contribution of current exoskeleton torque to torque on the next walking step is governed by the magnitude of the gain k_3 and provides negative force feedback. This term was included for two main reasons. First, it acts as a leaking term, slowly lessening the contribution of older coordination patterns to the current exoskeleton torque pattern. Second, it helps stabilize the system by defining an equilibrium criterion. Assuming the user maintains ankle kinematics and tibialis anterior muscle activity similar to baseline, this term defines a steady-state torque for a given reduction in soleus muscle activity. This prevents torque from growing unbounded. Additional details about the steady-state criteria of the algorithm, given the chosen gains, are

This article has been accepted for publication in a future issue of this journal, but has not been fully edited. Content may change prior to final publication. Citation information: DOI 10.1109/TNSRE.2019.2936383, IEEE Transactions on Neural Systems and Rehabilitation Engineering

provided in Appendix B. Finally, a deadband on the change in torque, $\max(|d\tau_{\text{des}}(i,n)| - d\tau_{\text{db}}, 0)$, sets sufficiently small values of $d\tau_{\text{des}}$ to zero to prevent desired exoskeleton torque from drifting upward due to non-zero baseline soleus muscle activity. The following formulation of the control scheme was implemented to best realize the driving heuristics:

$$\begin{aligned}&\tau_{\text{des}}(i,n+1) = \\ &\tau_{\text{des}}(i,n) + \text{sgn}(d\tau_{\text{des}}(i,n)) \cdot \max(|d\tau_{\text{des}}(i,n)| - d\tau_{\text{db}}, 0)\end{aligned} \tag{1}$$

where

$$\begin{aligned}&d\tau_{\text{des}}(i,n) = \\ &k_1 \cdot EMG_{\text{s}}(i+d,n) \cdot \langle EMG_{\text{s}}(n)\rangle^{-m} \\ &- k_2 \cdot EMG_{\text{t}}(i+d,n) - k_3 \cdot \tau_{\text{des}}(i,n) \\ &- k_4 \cdot \text{sgn}(\langle e_{\theta_{\text{a}}}(n)\rangle) \cdot \max(|\langle e_{\theta_{\text{a}}}(n)\rangle| - c_{\theta_{\text{a}}}, 0)\end{aligned} \tag{2}$$

The step number, n, was updated every heel strike and the time index, i, was updated at a frequency of 500 Hz. The desired exoskeleton torque profile, therefore, had a resolution of approximately 350 nodes, for a typical stance period of 700 ms for normal human gait. Through pilot testing, the constants were determined to be: $d = 84$ ms, $k_1 = 0.0025$ N·m·kg^{-1} · body mass, $k_2 = 0.05$ N·m, $k_3 = 0.01$, $k_4 = 2$ N·m·deg^{-1}, $m = 1.3$, $c_{\theta_{\text{a}}} = 5$ deg, and $d\tau_{\text{db}} = 0.01$ N·m.

To provide intuition for how the algorithm works, we examine calculations of torque at three different stages in the evolution. On the first walking step, torque from the exoskeleton is zero, soleus and tibialis anterior muscle activity are at normal levels, and ankle kinematics have not deviated from baseline. The change in torque is, therefore, the sum of the positive contribution from soleus muscle activity and the smaller negative contribution from tibialis anterior muscle activity, resulting in a net increase in torque. On the next walking step, exoskeleton torque is a small but non-zero value, soleus and tibialis anterior muscle activity remain close to normal levels, and ankle kinematics are similar to baseline. The change in torque is now the sum of the positive contribution from the soleus, the small negative contribution from the tibialis anterior, and the small negative contribution from the force feedback term. This combination similarly results in a net increase in torque. After a few minutes, exoskeleton torque begins inducing measurable changes in the user's coordination patterns. Soleus muscle activity is lower than baseline but still quite active, tibialis anterior muscle activity may have increased slightly, and ankle kinematics have likely started deviating outside the defined deadband. The change in torque is now the sum of the positive contribution from the soleus and the negative contributions from the tibialis anterior, ankle angle deviations, and the force feedback term. The net result is still a positive change in torque, but the magnitude of the change is small due to larger negative contributions. That is, the growth rate is slowing. After tens of minutes of walking, torque has likely reached an equilibrium point, in which the positive contribution from soleus muscle activity is offset by the negative contributions.

B. Algorithm Implementation

Measurements taken from two wired, bipolar electrodes (Bagnoli Desktop System, Delsys Inc., Boston, Massachusetts, USA) placed on the medial and lateral aspects of the soleus were averaged to give a single soleus muscle activity signal, EMG_{s}. Soleus muscle activity was high-pass filtered with a cutoff frequency of 20 Hz, full-wave rectified, low-pass filtered with a cut-off frequency of 6 Hz [21], [27], normalized to average peak muscle activity measured during walking while the exoskeletons applied zero torque, and shifted by the experimentally-determined delay every walking step. Average soleus muscle activity was calculated by integrating the normalized, non-delayed signal of soleus muscle activity over the current walking step using the trapezoidal method. Tibialis anterior muscle activity, EMG_{t}, was measured using one, bipolar electrode placed on the belly of the muscle. The signal was high-pass filtered with a cutoff frequency of 20 Hz, full-wave rectified, low-pass filtered with a cut-off frequency of 6 Hz [21], [27], normalized to average peak muscle activity measured during walking while the exoskeletons applied zero torque, and shifted by the experimentally-determined delay factor every walking step. Ankle angle was measured online using an absolute magnetic encoder placed at the ankle joint of the exoskeleton and low-pass filtered with a cut-off frequency of 50 Hz. The ankle angle profile over the dorsiflexion phase of gait on each walking step was subtracted from the dorsiflexion ankle angle profile during walking with 5 N·m of exoskeleton torque applied constantly throughout stance. The calculated difference at each time point was then averaged to obtain the ankle angle deviation term, $\langle e_{\theta_{\text{a}}}\rangle$. Additional details about the measurement of baseline ankle kinematics are provided in Appendix D.

C. Ankle Exoskeleton Emulator

The algorithm was implemented on a set of bilateral ankle exoskeletons via our emulator system which uses off-board motors and control architecture to actuate the exoskeleton end-effectors via a flexible tether (Fig. 3). The exoskeletons contacted the user at the shank below the knee via a strap worn around the calf, at the toe via a plate embedded in the front of the shoe, and at the heel via a rope embedded in the rear of the shoe (Fig. 9). Additional information about the exoskeleton end-effectors used in this study are provided in Appendix C. Full details of the emulator and ankle exoskeleton end-effectors can be found in [28], [29]. Control of the ankle exoskeletons was state-dependent, with different control methods used for the stance and swing phases of gait. During stance, torque control with iterative learning [30] was used to track the time-based, desired exoskeleton torque profile. During swing, motor position control was used to track the exoskeleton ankle joint angle with a defined amount of slack in the Bowden cable so as to not interfere with the natural motion of the user's ankle.

III. Evaluation of Controller Performance

We conducted an experiment to evaluate the effectiveness of the algorithm at discovering exoskeleton torque profiles that reduced metabolic rate in naïve exoskeleton users. Participants walked for 30 minutes with the co-adaptive controller as it

This article has been accepted for publication in a future issue of this journal, but has not been fully edited. Content may change prior to final publication. Citation information: DOI 10.1109/TNSRE.2019.2936383, IEEE Transactions on Neural Systems and Rehabilitation Engineering

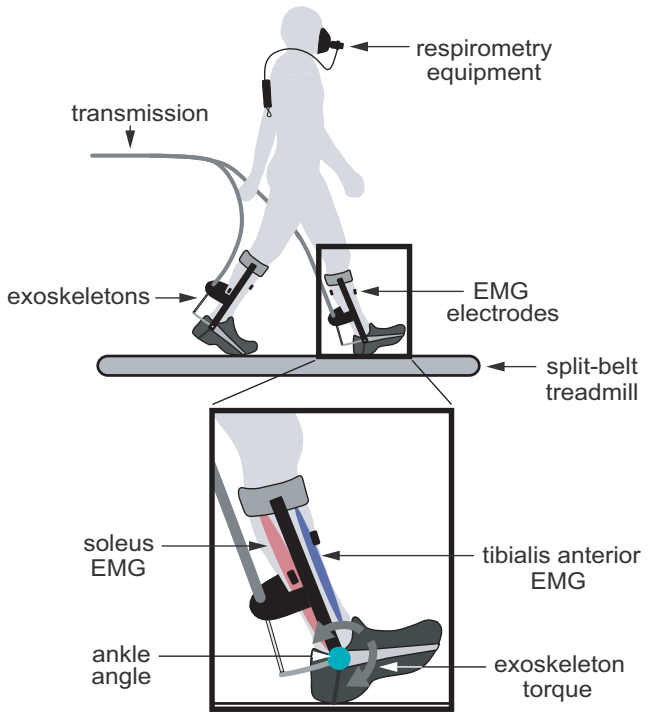

Fig. 3. Experimental set-up. Participants walked on an instrumented split-belt treadmill while wearing exoskeleton end-effectors on both legs. Flexible transmissions connected the exoskeletons to off-board motor and control hardware. EMG electrodes placed on the participants legs were used to measure muscle activity, while respirometry equipment was used to measure oxygen consumption and carbon dioxide expulsion. *Inset:* Soleus muscle activity, tibialis anterior muscle activity, ankle joint angle, and exoskeleton torque were continuously measured to update the co-adaptive controller and to be compared across conditions.

evolved based on the described heuristics (Adaptive). We measured soleus muscle activity and whole-body metabolic rate to observe how changes in muscle activity patterns affected torque profiles and how the torque profiles affected muscle activity patterns and whole-body coordination strategies. We compared these outcomes to those measured during walking with a static torque profile (Static) to give context to the results from the Adaptive condition. This Static profile was defined as the average of participant-optimized torque profiles from a different protocol [6], in which each participant's torque profile was optimized to directly minimize metabolic rate. The shape of the Static profile was the same for each participant, with the magnitude normalized by body mass. The goal was for the co-adaptive controller to match improvements in metabolic rate achieved with the Static torque profile. All outcomes were reported in reference to a baseline condition defined as walking with bilateral exoskeletons as they provided zero torque (Zero Torque). Finally, to capture the added cost of wearing the exoskeletons, we compared the Zero Torque condition to walking in normal shoes (Normal Walking).

A. Experimental Protocol

Ten able-bodied individuals (8 men and 2 women; age = 22.7 $\pm$ 2.0 yrs; body mass = 68.3 $\pm$ 9.4 kg; height = 1.75 $\pm$ 0.05 m) participated in the study. No participants had worn the exoskeletons prior to the study and all participants provided written informed consent before completing the protocol approved by the Carnegie Mellon Institutional Review Board.

The Adaptive and Static conditions each consisted of one 30-minute trial. The presentation of the Adaptive and Static conditions was randomized to account for ordering and learning effects. The Normal Walking condition consisted of one six-minute trial and was randomly chosen to come either first or last. The Zero Torque condition was the average of two, six-minute trials in which the exoskeletons were worn on both ankles but provided zero torque. One trial was performed before the Adaptive and Static conditions and one trial was performed after. All walking trials were performed on a treadmill at 1.25 m·s^{-1}. Basal metabolic rate was obtained through a Quiet Standing condition lasting four minutes. Additional details about the experimental protocol are provided in Appendix D.

B. Measured Outcomes

1) Muscle Activity: Muscle activity was measured using surface electromyography and processed as described previously. Average peak and root-mean-square (RMS) of the processed electromyography signals were calculated for the last three minutes of each walking condition and used to compare muscle activity across the different conditions.

2) Metabolic Rate: Metabolic rate was estimated by substituting volumetric oxygen consumption and carbon dioxide expulsion flow rates into a widely-used equation [31]. Volumetric flow rates were measured using indirect calorimetry via a portable metabolics cart (Oxycon Mobile, CareFusion, San Diego, California, USA). The average of the last three minutes of metabolics data for each condition, normalized to body mass, was used as our measure of steady-state metabolic rate. Net metabolic rate was calculated by subtracting the metabolic rate of Quiet Standing from the different walking conditions. Change in metabolic rate was calculated by subtracting net metabolic rate of each walking condition from net metabolic rate of the Zero Torque condition.

3) Exoskeleton Mechanics: We used on-board sensors to measure ankle exoskeleton kinematics and kinetics. Exoskeleton ankle joint angle was measured using an absolute magnetic encoder, sampled at 500 Hz and low-pass filtered with a cut-off frequency of 50 Hz. Exoskeleton plantarflexion torque was measured using calibrated strain gauges, sampled at 500 Hz and low-pass filtered with a cut-off frequency of 50 Hz. The desired exoskeleton torque profile was averaged over the last three minutes of the Adaptive condition and normalized to body mass. Average peak and RMS of the evolved exoskeleton torque profiles were calculated for the last three minutes of the Adaptive condition for the left and right legs independently. These measures were used to compare the evolved torque profiles across legs and subjects and to the torque profile applied in the Static condition.

4) Separation into Strides: Ground reaction forces, sampled at a frequency of 500 Hz using an instrumented split-belt treadmill (Bertec, Columbus, Ohio, USA) and low-pass filtered with a cut-off frequency of 60 Hz, were used to detect

This article has been accepted for publication in a future issue of this journal, but has not been fully edited. Content may change prior to final publication. Citation information: DOI 10.1109/TNSRE.2019.2936383, IEEE Transactions on Neural Systems and Rehabilitation Engineering

the swing and stance phases of gait. A threshold of 150 N was used to trigger heel-strike and toe-off. All time-trajectories of interest were separated into strides.

5) Statistical Analysis: We compared soleus muscle activity, exoskeleton torque, and metabolic rate across walking conditions. Average trajectories, normalized to percent stride, were generated for each subject. All outcomes were averaged across subjects. Standard deviations represent variations between subjects. We performed paired t-tests to compare results across the two conditions of interest for a given outcome. We then applied the Holm-Šídák step-down correction for multiple comparisons [32] and used a significance level of $\alpha = 0.05$.

IV. Results

We developed a heuristic-based algorithm that uses measurements of muscle activity and joint kinematics to drive the evolution of a desired exoskeleton torque profile. We conducted an experiment to evaluate the effectiveness of the algorithm and found that the resulting growth in exoskeleton torque led to significant reductions in soleus muscle activity and whole-body metabolic rate.

A. Evolved Torque Profiles and Reductions in Soleus EMG

The co-adaptive controller resulted in slow growth of exoskeleton torque, guided by changes in measured soleus muscle activity, tibialis anterior muscle activity, and ankle kinematics, which led to a coincident reduction in soleus muscle activity (Fig. 2). Exoskeleton torque evolved independently for the left and right legs and for each participant, resulting in different torque profiles between limbs and across participants (Fig. 4A). On average, RMS of exoskeleton torque was 0.32 ± 0.058 N·m·kg^{-1} and peak exoskeleton torque was 0.75 ± 0.21 N·m·kg^{-1}. Soleus muscle activity, particularly during late stance, was significantly reduced when participants walked with the co-adaptive exoskeleton controller. Average RMS and peak soleus muscle activity in the Adaptive condition were 32.6% and 56% lower, respectively, compared to the Zero Torque condition ($p = 3 \cdot 10^{-6}$ and $p = 3 \cdot 10^{-6}$, respectively, Fig. 4B). Reductions in RMS soleus muscle activity ranged from 15% to 54%.

B. Reductions in Whole-Body Metabolic Rate

The algorithm we developed led to substantial reductions in metabolic rate below walking in the Zero-Torque mode and below walking in normal shoes, comparable to reductions achieved with the previously-optimized static exoskeleton torque profile (Fig. 5). Metabolic rate decreased, on average, from 3.43 ± 0.51 W·kg^{-1} in the Zero Torque condition to 2.66 ± 0.38 W·kg^{-1} in the Adaptive condition, a 22.0% reduction ($p = 1 \cdot 10^{-4}$). Reductions in metabolic rate ranged from 12.1% to 40.0% across participants. Compared to Normal Walking, the co-adaptive exoskeleton controller reduced metabolic rate by 8.7%. Net metabolic rate was not significantly different across the Adaptive and Static conditions ($p = 0.8$).

Discussion

Soleus muscle activity, tibialis anterior muscle activity, and ankle joint kinematics guided the evolution of ankle exoskeleton torque profiles that effectively reduced whole-body metabolic rate. Average metabolic savings, compared to walking in the Zero-Torque mode, amounted to 22.0%, which is approximately equivalent to removing a 33 lb backpack [33]. Such reductions were achieved within 30 minutes and did not incorporate direct measurements of metabolic rate into the update law.

The co-adaptive control strategy led to greater reductions in soleus muscle activity and metabolic energy consumption in less time than alternative electromyography-driven approaches. Traditional proportional myoeletric control only reduced soleus muscle activity by 26% and metabolic rate by 8%, compared to walking with the exoskeletons turned off [21]. Adding an adaptive gain to the proportional myoelectric controller resulted in even smaller reductions in soleus muscle activity but improved reductions in metabolic rate [34]; the metabolic cost savings were consistent with those achieved in the current study. In the above-referenced experiments, participants were given three 30-minute trials of walking with the respective controller, three times the exposure provided in the current study. The co-adaptive control strategy was able to achieve equivalent gains in less time, demonstrating its effectiveness.

One major benefit of the co-adaptive control strategy is its ability to continuously respond to the user over time. The shape of the assistance profile changed as soleus muscle activity patterns changed and the growth of the assistance profile slowed down when coordination strategies deviated significantly from normal walking (Movie 1). Although most significant changes in torque magnitude happened during the first couple of minutes of walking with the co-adaptive controller, subtler changes in the shape of the torque pattern continued throughout the 30-minute Adaptive condition (Fig. 6A, Movie 1), indicating that users were still changing their coordination patterns. Furthermore, average metabolic rate was still decreasing at the end of the 30-minute condition, suggesting the potential for further gains with continued exposure to this controller (Fig. 6B). More testing is required to explore this idea.

A second major benefit of the co-adaptive control strategy is its ability to quickly identify effective, high-dimensional assistance profiles for new devices. The algorithm can realize any pattern of torque governed by measured muscle activity. Although the current implementation of the algorithm is relatively device-specific, modified versions of the algorithm will likely generalize to other joints. For example, by expanding measurements of muscle activity and joint kinematics to cover the entire gait cycle, torque can be adjusted during both the stance and swing phases of gait. Additionally, to incorporate bi-directional control of a device, such as flexion and extension, incorporating average muscle activity contributions for both the flexor and extensor muscles will likely be necessary, and the gains on these different muscle contributions will need to be adjusted to achieve the appropriate relative

This article has been accepted for publication in a future issue of this journal, but has not been fully edited. Content may change prior to final publication. Citation information: DOI 10.1109/TNSRE.2019.2936383, IEEE Transactions on Neural Systems and Rehabilitation Engineering

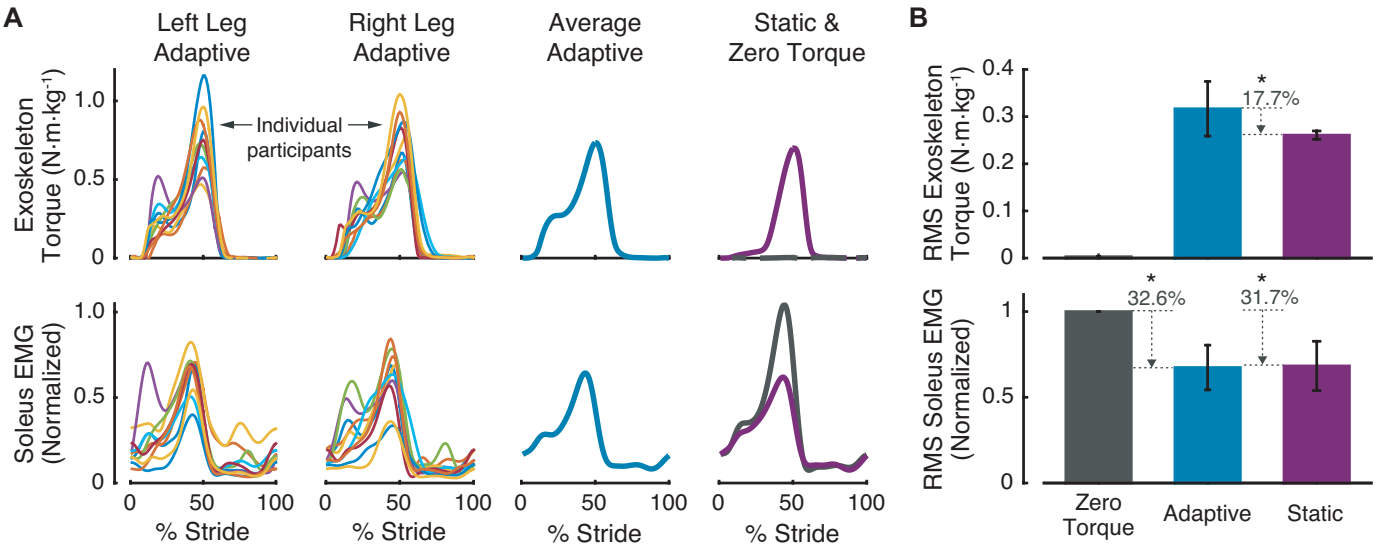

Fig. 4. The co-adaptive controller led to evolved torque profiles that varied between legs and across participants and significantly reduced soleus muscle activity below that measured during walking in the Zero-Torque mode. (A) Exoskeleton torque profiles (*top*) and soleus muscle activity profiles (*bottom*) averaged over the last three minutes of walking in each condition. *From left to right:* Profiles for the left leg for each participant walking with the co-adaptive controller; profiles for the right leg for each participant walking with the co-adaptive controller; participant- and leg-averaged profiles for walking with the co-adaptive controller; participant- and leg-averaged profiles during walking with the static controller (purple) and in the Zero-Torque mode (grey). (B) RMS of exoskeleton torque (*top*) and soleus muscle activity (*bottom*) during walking in the Zero-Torque mode (Zero Torque), during walking with the co-adaptive controller (Adaptive), and during walking with a static controller (Static). The Static controller is the best known controller to date, taken as the average of participant-optimized torque profiles from a different protocol [6]. Bars are means and error bars are standard deviations due to intersubject variability. Asterisks indicate statistical significance ($p < 0.05$).

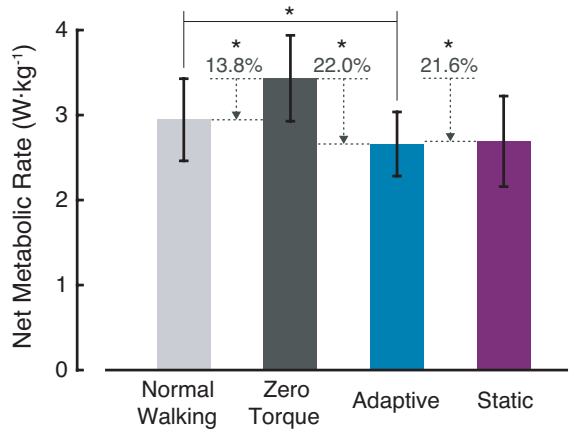

Fig. 5. Metabolic rate across different conditions. The co-adaptive controller (Adaptive) significantly reduced metabolic rate below walking in the Zero-Torque mode (Zero Torque) and below walking in normal shoes (Normal Walking). Similar reductions in metabolic rate were observed during walking with a static torque profile (Static). Bars are means and error bars are standard deviations due to intersubject variability. Asterisks indicate statistical significance ($p < 0.05$).

flexion/extension moments. Further adjustment of control parameters could be performed to decrease or increase the rate of change of the assistance profile for different populations and different devices.

Finally, a third major benefit of the co-adaptive control strategy is its ability to scale well to multiple joints. Many direct optimization methods scale at least linearly, if not exponentially, with the number of parameters [23], [35], [36]. Covariance matrix adaptation evolutionary strategies (CMAES) do slightly better, theoretically scaling with the log of the number of parameters [30]. Bayesian optimization can also improve sampling efficiency, but is subject to the curse of dimensionality and becomes computationally unwieldy at around 10 parameters [37]. With this heuristic-based algorithm, adding control over an additional joint is equivalent to adding just one computation at every time step. We showed this capability by independently applying the controller to bilateral exoskeletons, requiring the algorithm to separately discover torque profiles for the left and right legs. Given the aforementioned strengths, effective generalization and scaling of this approach could lay the foundation for a full lower-limb exoskeleton assistance strategy.

The current formulation of the controller may benefit from adjustments to its implementation. The desired torque profile was restricted to converge to a neighborhood of the average pattern of soleus muscle activity, assuming only small increases in tibialis anterior muscle activity (Fig. 8), due to the inclusion of a negative gain on the desired torque. Replacing this term with a gross measure of torque, such as average torque or peak torque, or another generic stabilizing term could remove this constraint and enable the discovery of a broader range of assistance profiles, some of which may prove more effective. The constants used in the algorithm were determined through experimental testing. Future work should include a rigorous characterization of the control parameters and their allowable bounds. Optimization of these constants could result in assistance profiles that elicit even more beneficial interactions between the device and user.

Heuristic-based controllers inherently rely on assumptions and intuition that may be imperfect or incorrect, which is a

This article has been accepted for publication in a future issue of this journal, but has not been fully edited. Content may change prior to final publication. Citation information: DOI 10.1109/TNSRE.2019.2936383, IEEE Transactions on Neural Systems and Rehabilitation Engineering

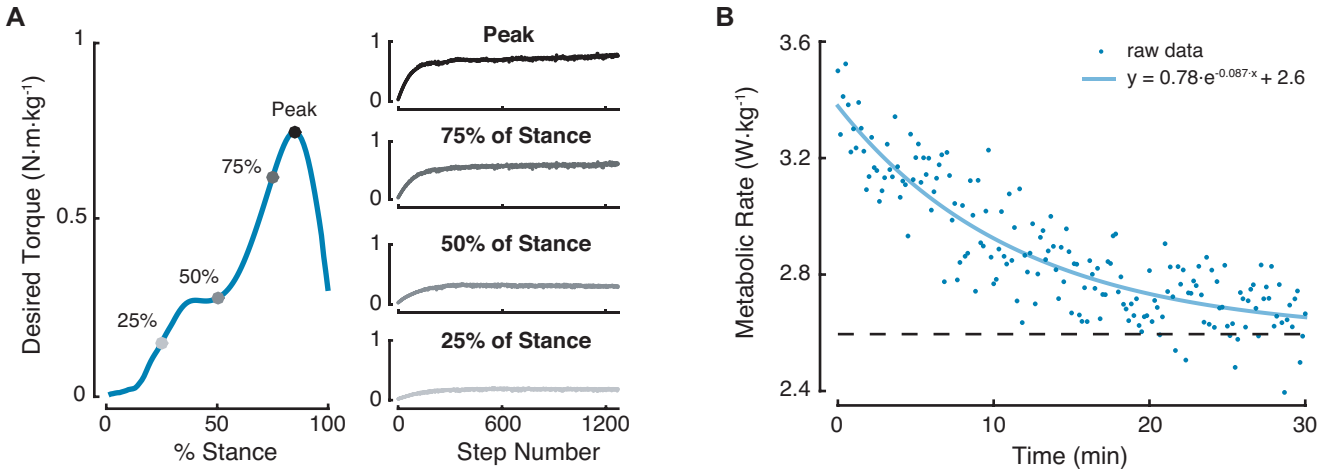

Fig. 6. (A) Exoskeleton torque over time, averaged across subjects and legs, reach steady state. *Left:* The blue curve shows exoskeleton torque on the last walking stride of the Adaptive condition, as a percent of stance. The dots on the trajectory indicate torque at 25% of stance, 50% of stance, 75% of stance, and peak torque. *Right:* The subplots show the evolution of, from top to bottom, peak torque, torque at 75% of stance, torque at 50% of stance, and torque at 25% of stance over time, as a function of step number. Most magnitude changes in the torque pattern happened, on average, within the first four minutes of the Adaptive condition. Changes in the shape of the torque pattern continued throughout the remainder of the condition. (B) Subject-averaged metabolic rate over time and exponential fit. Metabolic rate decreased exponentially over the 30-minute walking trial in the Adaptive condition, but did not, on average, reach steady state by the end of the trial. The blue dots are raw data averaged across subjects, normalized to body mass. The blue line is an exponential fit to the raw data.

concern for the presented controller. For example, it remains unclear whether incorporating memory into the controller is beneficial. Furthermore, the controller penalizes large kinematic changes, even though the relationship between metabolic energy reductions and kinematic adaptations has not been well characterized. These decisions were made based on previous experience developing assistance strategies. We attempted to balance natural kinematic adaptations to exoskeleton torque with excessive kinematic adaptations, and guide users towards reducing soleus muscle activity instead of only changing kinematics. Additional testing of the size of the deadband and the value of the gain on the kinematic error term could be performed to better characterize the effect of kinematic constraints on the evolved torque profile and the user's whole-body metabolic rate.

Continued lab-based research is necessary before this control approach is ready to be deployed on commercial exoskeletons. Experiments were performed on a treadmill, at steady-state, thus, it remains to be seen how this controller will perform in more ecological scenarios, such as variable speed or inclined walking. Applying this control approach to exoskeletons acting about more complex joints, e.g. the hip joint, may prove challenging given the inherent limitations of measuring muscle activity using surface electromyography. Some superficial muscles are, however, still available. Furthermore, electromyography sensors can be cumbersome, but they are still more mobile than metabolic carts and many companies are working on developing more robust, wearable electromyography systems.

Although this control approach worked well for able-bodied individuals, it will likely not be effective for populations with altered muscle activity, such as amputees or individuals post-stroke. The evolved assistance profiles are dependent on patterns of muscle activity, therefore torque profiles could not be generated from an amputated limb or a limb with abnormal muscle activity due to neurological injury. The primary candidates for assistance with this control strategy are those with generally normal patterns of muscle activity but reduced muscle strength, including the 18% of adults over the age of 60 with muscle weakness [38] and any other individuals scoring less than five on the Medical Research Council (MRC) muscle strength scale [39]. Exoskeleton torque profiles could still evolve based upon measured muscle activity with such individuals, and the resulting assistance may help compensate for any reduced functionality caused by muscle weakness.

V. Conclusion

We developed a heuristic-based algorithm to simultaneously adapt to changes in each user's coordination patterns and discover individualized exoskeleton assistance strategies that effectively improve locomotor economy. Soleus muscle activity, tibialis anterior muscle activity, and ankle joint kinematics, measured online, were used to guide the evolution of an exoskeleton torque profile. The algorithm led to exoskeleton torque profiles that substantially reduced soleus muscle activity and whole-body metabolic rate in naïve exoskeleton users, showing the effectiveness of the approach. This control approach can quickly identify high-dimensional assistance patterns and is tolerant of, and responsive to, slow user adaptation. We expect this co-adaptive algorithm to enable the discovery of effective lower-limb assistance strategies for able-bodied individuals and those with muscle weakness, such as the elderly, especially in complex paradigms.

This article has been accepted for publication in a future issue of this journal, but has not been fully edited. Content may change prior to final publication. Citation information: DOI 10.1109/TNSRE.2019.2936383, IEEE Transactions on Neural Systems and Rehabilitation Engineering

APPENDIX A
EVOLVED TARGET VARIABLES

To facilitate comparisons of this controller to previous research, we provide subject-averaged trajectories for each component included in the controller and bar plots of metrics of interest for each respective component (Fig. 7).

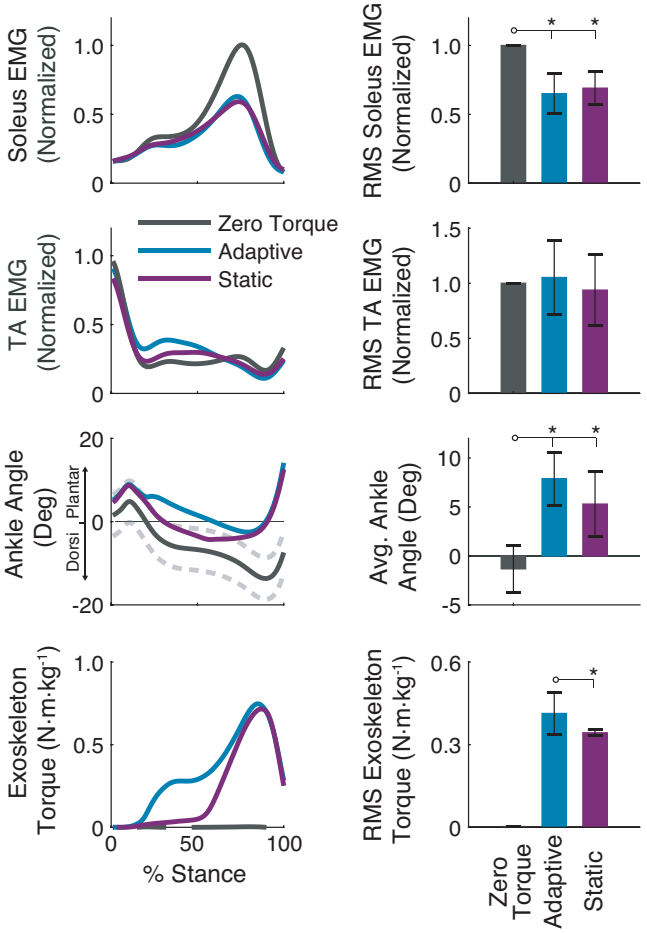

Fig. 7. Subject-averaged evolved target variables. *Left column from top to bottom:* Soleus muscle activity, tibialis anterior (TA) muscle activity, ankle kinematics, and exoskeleton torque profiles as a percent of stance averaged over the last three minutes of walking in the Zero Torque condition (grey), the Adaptive condition (blue), and the Static condition (purple). The dashed grey lines depict the deadband around baseline ankle kinematics included in the controller. *Right column from top to bottom:* RMS of soleus muscle activity, RMS of tibialis anterior muscle activity, average ankle angle, and RMS of exoskeleton torque. Bars are means and error bars are standard deviations due to intersubject variability. Asterisks indicate statistical significance ($p < 0.05$).

APPENDIX B
STEADY-STATE TORQUE

The inclusion of a negative force feedback term, $-k_3 \cdot \tau_{\text{des}}$, in the heuristic-based algorithm constrained steady-state torque (τ_{ss}) to be

$$\begin{aligned}\tau_{\text{ss}} =& k_1 \cdot k_3^{-1} \cdot EMG_{\text{s}} \cdot \langle EMG_{\text{s}}(n) \rangle^{-m} \\ &- k_2 \cdot k_3^{-1} \cdot EMG_{\text{t}} \\ &- k_4 \cdot k_3^{-1} \cdot \text{sgn}(\langle e_{\theta_{\text{a}}}(n) \rangle) \pm d\tau_{\text{db}} \cdot k_3^{-1}\end{aligned} \tag{3}$$

where k_1, k_2, k_3, k_4, m, $c_{\theta_{\text{a}}}$, and $d\tau_{\text{db}}$ are experimentally-determined constants.

The relative values of k_1 and k_3 defined the steady-state torque for a given reduction in soleus muscle activity, assuming minimal to no contributions from the tibialis anterior and ankle kinematics terms. This criteria restricted the shape of the steady-state torque profile to a neighborhood of the soleus muscle activity pattern (Fig. 8).

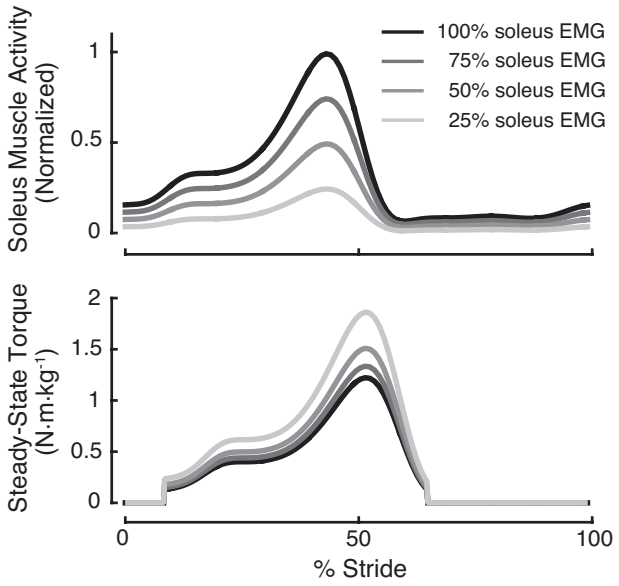

Fig. 8. Exoskeleton torque profile at steady state for a theoretical reduction in soleus muscle activity. *Top:* Theoretical reductions in soleus muscle activity. 100% soleus muscle activity is equivalent to baseline muscle activity during walking in the Zero-Torque mode. Additional trajectories are theoretical reductions in soleus muscle activity, in which the entire trajectory is scaled down by a constant factor, ranging from 75% of baseline soleus muscle activity to 25% of baseline muscle activity. This type of scaling similarly affects average soleus muscle activity. Non-uniform changes in muscle activity are, however, possible, and were more commonly observed during the experiment *Bottom:* Steady-state torque for a theoretical reduction in soleus muscle activity, given baseline tibialis anterior muscle activity, no change in ankle kinematics, and no deadband around the change in desired torque. Larger reductions in soleus muscle activity, as defined here, converge to larger steady-state torque. Steady-state torque was restricted to be within a neighborhood of the pattern of soleus muscle activity.

APPENDIX C
ANKLE EXOSKELETON EMULATOR

External plantarflexion torque was applied about both ankles using our ankle exoskeleton emulator (Fig. 9), the details of which are provided in [28], [29]. The ankle exoskeleton end-effectors contacted the user at three places on the body: at the shank below the knee, under the ball of the shoe, and under the heel of the shoe. Each end-effector had a mass of 0.875 kg and was actuated by a powerful off-board motor, with forces transmitted through a flexible, unidirectional Bowden cable tether. The end-effectors had rotational joints on the medial and lateral sides of each leg, with the axis of rotation approximately aligned with the center of the user's lateral malleolus.

This article has been accepted for publication in a future issue of this journal, but has not been fully edited. Content may change prior to final publication. Citation information: DOI 10.1109/TNSRE.2019.2936383, IEEE Transactions on Neural Systems and Rehabilitation Engineering

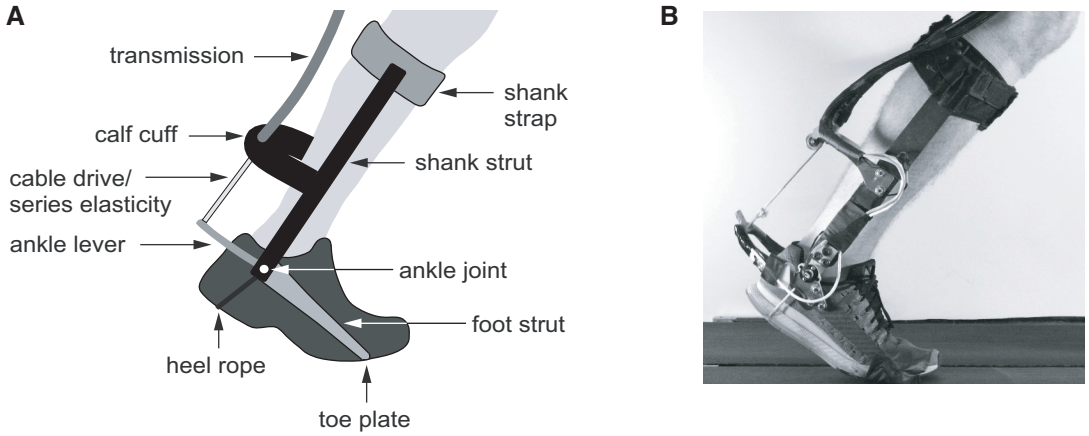

Fig. 9. Ankle exoskeleton end-effector used during experiments. (A) Schematic of the exoskeleton end-effector with major components identified. Additional information about the exoskeletons can be found in [29]. (B) Photograph of the exoskeleton end-effector.

The exoskeleton end-effectors were instrumented to measure device mechanics and trigger state transitions. Exoskeleton plantarflexion torque was measured with four strain gages (MMF003129, Micro Measurements, Wendell, NC, USA) affixed to the frame in a Wheatstone bridge configuration. Root-mean-square error of measured torque was 0.125 N·m, or 0.25% of peak [29]. Exoskeleton joint angle was measured using an absolute magnetic encoder (MAE3, US Digital, Vancouver, Washington, USA) mounted on the lateral side of each exoskeleton's ankle joint. Foot contact was detected using a pressure switch (McMaster-Carr, Aurora, Ohio, USA) situated in the heel of each shoe.

Control of the ankle exoskeletons was dependent on the phase of the gait cycle. During stance, the desired exoskeleton torque-time pattern was tracked using torque control. Exoskeleton torque control was achieved using a combination of proportional control, damping injection, and iterative learning compensation. This method of torque control was previously shown to result in torque tracking errors as low as 1% of the peak torque during walking, which is lower than the torque tracking errors observed with other commonly used torque control methods [30]. During swing, exoskeleton ankle joint angle was tracked using motor position control. A defined length of slack was maintained in the Bowden cable to reduce interference with the user's natural ankle motion. The ankle exoskeleton emulator was capable of generating peak plantarflexion moments during walking of approximately 120 N·m [29].

Appendix D
Additional Experimental Details

The soleus muscle activity terms, EMG_s and $\langle EMG_s \rangle$, and the tibialis anterior muscle activity term, EMG_t, in the co-adaptive controller were normalized to peak baseline soleus and tibialis anterior muscle activity, respectively. Baseline muscle activity was measured just prior to the start of the 30-minute Adaptive condition. Participants walked on the treadmill at 1.25 m·s^{-1} for 30 consecutive steps in the Zero-Torque mode while we measured soleus and tibialis anterior muscle activity. We then averaged each of these muscle activity profiles and defined the peaks of these average profiles as our normalization factors.

The deviation in ankle kinematics term, e_{θ_a}, in the co-adaptive controller was defined as the average difference between measured and nominal ankle angle profiles at each point in time, over the dorsiflexion phase of gait. Nominal ankle kinematics were measured immediately after measuring baseline muscle activity. Participants walked on the treadmill at 1.25 m·s^{-1} while the exoskeleton applied a constant torque of 5 N·m throughout the stance phase of gait. This small, but imperceptible, amount of torque was meant to account for shifting of the exoskeleton on the leg when forces were transmitted through the bowden cable. Specifically, we did not want changes in ankle kinematics due purely to shifting of the exoskeleton to contribute to changes in the desired torque profile. We let the user to walk for approximately 30 seconds with the 5 N·m square-wave of torque to allow iterative learning to compensate for any large torque-tracking errors. Once we determined, through visual inspection, that desired torque was being tracked well, we measured ankle kinematics over 30 consecutive steps, then averaged these trajectories to obtain a nominal ankle angle trajectory. We then briefly put the exoskeleton back into the Zero-Torque mode, updated the co-adaptive controller with the computed nominal values, then started the Adaptive condition in which exoskeleton torque evolved as defined by the heuristic-based algorithm.

Acknowledgment

The authors would like to thank C. Morales and T. Nguyen for help with data collections.

References

[1] P. Malcolm, W. Derave, S. Galle, and D. De Clercq, "A simple exoskeleton that assists plantarflexion can reduce the metabolic cost of human walking," *PLoS: ONE*, vol. 8, p. e56137, 2013.

[2] L. M. Mooney, E. J. Rouse, and H. M. Herr, "Autonomous exoskeleton reduces metabolic cost of human walking," *J. Neuroeng. Rehabil.*, vol. 11, p. 151, 2014.

[3] S. H. Collins, M. B. Wiggin, and G. S. Sawicki, "Reducing the energy cost of human walking using an unpowered exoskeleton," *Nature*, vol. 522, pp. 212–215, 2015.

[4] J. R. Koller, D. A. Jacobs, D. P. Ferris, and C. D. Remy, "Learning to walk with an adaptive gain proportional myoelectric controller for a robotic ankle exoskeleton," *J. Neuroeng. Rehabil.*, vol. 12, p. 97, 2015.

[5] K. Seo, J. Lee, Y. Lee, T. Ha, and Y. Shim, "Fully autonomous hip exoskeleton saves metabolic cost of walking," in *Proc. Int. Conf. Rob. Autom.*, 2016, pp. 4628–4635.

[6] J. Zhang, P. Fiers, K. A. Witte, R. W. Jackson, K. L. Poggensee, C. G. Atkeson, and S. H. Collins, "Human-in-the-loop optimization of exoskeleton assistance during walking," *Science*, vol. 356, no. 6344, pp. 1280–1284, 2017.

[7] B. T. Quinlivan, S. Lee, P. Malcolm, D. M. Rossi, M. Grimmer, C. Siviy, N. Karavas, D. Wagner, A. Asbeck, I. Galiana, and C. J. Walsh, "Assistance magnitude versus metabolic cost reductions for a tethered multiarticular soft exosuit," *Science Robotics*, vol. 2, p. eaah4416, 2017.

[8] S. Galle, W. Derave, F. Bossuyt, P. Calders, P. Malcolm, and D. D. Clercq, "Exoskeleton plantarflexion assistance for elderly," *Gait Post.*, vol. 52, pp. 183–188, 2016.

[9] A. K. Raj, P. D. Neuhaus, A. M. Moucheboeuf, J. H. Noorden, and D. V. Lecoutre, "Mina: A sensorimotor robotic orthosis for mobility assistance," *Journal of Robotics*, vol. 2011, p. 284352, 2011.

[10] J.-B. Mignardot, C. G. L. Goff, R. van den Brand, M. Capogrosso, N. Fumeaux, H. Vallery, S. Anil, J. Lanini, I. Fodor, G. Eberle, A. Ijspeert, B. Church, A. Curt, S. Carda, J. Bloch, J. von Zitzewitz, and G. Courtine, "A multidirectional gravity-assist algorithm that enhances locomotor control in patients with stroke or spinal cord injury," *Sci. Transl. Med.*, vol. 9, p. eaah3621, 2017.

[11] S. Srivastava, P. C. Kao, S. H. Kim, P. Stegall, D. Zanotto, J. S. Higginson, S. K. Agrawal, and J. P. Scholz, "Assist-as-needed robot-aided gait training improves walking function in individuals following stroke," *Trans. Neural Syst. Rehabil. Eng.*, vol. 23, pp. 956–963, 2015.

[12] L. N. Awad, J. Bae, K. O'Donnell, S. M. M. D. Rossi, K. Hendron, L. H. Sloot, P. Kudzia, S. Allen, K. G. Holt, T. D. Ellis, and C. J. Walsh, "A soft robotic exosuit improves walking in patients after stroke," *Sci. Transl. Med.*, vol. 9, p. eaai9084, 2017.

[13] A. D. Kuo, "Energetics of actively powered locomotion using the simplest walking model," *J. Biomech. Eng.*, vol. 124, pp. 113–120, 2002.

[14] S. H. Collins and A. D. Kuo, "Recycling energy to restore impaired ankle function during human walking," *PLoS: ONE*, vol. 5, p. e9307, 2010.

[15] T. K. Uchida, A. Seth, S. Pouya, C. L. Dembia, J. L. Hicks, and S. L. Delp, "Simulating ideal assistive devices to reduce the metabolic cost of running," *PLoS: ONE*, vol. 11, p. e0163417, 2016.

[16] C. L. Dembia, A. Silder, T. K. Uchida, J. L. Hicks, and S. L. Delp, "Simulating ideal assistive devices to reduce the metabolic cost of walking with heavy loads," *PLoS: ONE*, vol. 12, p. e0180320, 2017.

[17] T. M. Griffin, T. J. Roberts, and R. Kram, "Metabolic cost of generating muscular force in human walking: insights from load-carrying and speed experiments," *J. Appl. Physiol.*, vol. 95, pp. 172–183, 2003.

[18] A. Grabowski, C. Farley, and R. Kram, "Independent metabolic costs of supporting body weight and accelerating body mass during walking," *J. Appl. Physiol.*, vol. 98, pp. 579–583, 2005.

[19] R. W. Jackson and S. H. Collins, "An experimental comparison of the relative benefits of work and torque assistance in ankle exoskeletons," *J. Appl. Physiol.*, vol. 119, pp. 541–557, 2015.

[20] K. E. Gordon and D. P. Ferris, "Learning to walk with a robotic ankle exoskeleton," *J. Biomech.*, vol. 40, pp. 2636–2644, 2007.

[21] G. S. Sawicki and D. P. Ferris, "Mechanics and energetics of level walking with powered ankle exoskeletons," *J. Exp. Biol.*, vol. 211, pp. 1402–1413, 2008.

[22] T. Lenzi, M. C. Carrozza, and S. K. Agrawal, "Powered hip exoskeletons can reduce the user's hip and ankle muscle activations during walking," *Trans. Neural Syst. Rehabil. Eng.*, vol. 21, pp. 938–948, 2013.

[23] J. R. Koller, D. H. Gates, D. P. Ferris, and C. D. Remy, "'body-in-the-loop' optimization of assistive robotic devices: A validation study," in *Robotics: Science and Systems*, 2016.

[24] Y. Ding, M. Kim, S. Kuindersma, and C. J. Walsh, "Human-in-the-loop optimization of hip assistance with a soft exosuit during walking," *Science Robotics*, vol. 3, p. eaar5438, 2018.

[25] J. C. Selinger, S. M. OConnor, J. D. Wong, and J. M. Donelan, "Humans can continuously optimize energetic cost during walking," *Current Biology*, vol. 25, no. 18, pp. 2452–2456, 2015.

[26] D. P. Ferris, K. E. Gordon, and G. S. Sawicki, "An improved powered ankle-foot orthosis using proportional myoelectric control," *Gait Post.*, vol. 23, pp. 425–428, 2006.

[27] C. J. De Luca, L. D. Gilmore, M. Kuznetsov, and S. H. Roy, "Filtering the surface emg signal: Movement artifact and baseline noise contamination," *J. Biomech.*, vol. 43, pp. 1573–1579, 2010.

[28] J. M. Caputo and S. H. Collins, "A universal ankle-foot prosthesis emulator for experiments during human locomotion," *J. Biomech. Eng.*, vol. 136, p. 035002, 2014.

[29] K. A. Witte, J. Zhang, R. W. Jackson, and S. H. Collins, "Design of two lightweight, high-bandwidth torque-controlled ankle exoskeletons," in *Proc. Int. Conf. Rob. Autom.*, 2015, pages 1223-1228.

[30] J. Zhang, C. C. Cheah, and S. H. Collins, *Torque control in legged locomotion. In Bio-Inspired Legged Locomotion: Concepts, Control and Implementation*, M. Sharbafi and A. Seyfarth, Eds. Butterworth-Heinemann, 2017, chapter 5, pp. 347-395.

[31] J. M. Brockway, "Derivation of formulae used to calculate energy expenditure in man," *Hum. Nutr. Clin. Nutr.*, vol. 41C, pp. 463–471, 1987.

[32] S. A. Glantz, *Primer of Biostatistics, Seventh Edition*. The McGraw-Hill Companies, Inc., 2012, 65.

[33] R. C. Browning, J. R. Modica, R. Kram, and A. Goswami, "The effects of adding mass to the legs on the energetics and biomechanics of walking," *Med. Sci. Sports Exer.*, vol. 39, pp. 515–525, 2007.

[34] J. R. Koller, C. D. Remy, and D. P. Ferris, "Biomechanics and energetics of walking in powered ankle exoskeleton using myoelectric control versus mechanically intrinsic control," *J. Neuroeng. Rehabil.*, vol. 15, p. 42, 2018.

[35] S. Galle, P. Malcolm, S. H. Collins, and D. D. Clercq, "Reducing the metabolic cost of walking with an ankle exoskeleton: interaction between actuation timing and power," *J. Neuroeng. Rehabil.*, vol. 14, no. 1, p. 35, 2017.

[36] W. Felt, J. C. Selinger, J. M. Donelan, and C. D. Remy, ""body-in-the-loop": Optimizing device parameters using measures of instantaneous energetic cost," *PLoS: ONE*, vol. 10, p. e0135342, 2015.

[37] M. Kim, Y. Ding, P. Malcolm, J. Speeckaert, C. J. Siviy, C. J. Walsh, and S. Kuindersma, "Human-in-the-loop bayesian optimization of wearable device parameters," *PLoS: ONE*, vol. 12, p. e0184054, 2017.

[38] A. C. Looker and C.-Y. Wang, "Prevalence of reduced muscle strength in older u.s. adults: United states, 2011-2012," *Women*, vol. 60, p. 79, 2015.

[39] M. R. Council, "Aids to the examination of the peripheral nervous system," *HM Stationary Office*, 1976.